

Two-dimensional MXene and molybdenum disulphide for the removal of hexavalent chromium from water: A comparative study



Asma Maqsood Abbasi^a, Waqas Qamar Zaman^{a,b}, Hassan Anwer^a, Fahad Azad^c, Xizi Long^d, Waheed Miran^{e,*}, Musharib Khan^{a,*}

^a Institute of Environmental Sciences and Engineering, School of Civil and Environmental Engineering, National University of Sciences and Technology (NUST), Sector H-12, Islamabad 44000, Pakistan

^b Department of Civil and Environmental Engineering, Hong Kong Polytechnic University, Hung Hom, Hong Kong

^c School of Natural Sciences (SNS), National University of Sciences and Technology (NUST), Islamabad 44000, Pakistan

^d The Key Laboratory of Typical Environmental Pollution and Health Hazards of Hunan Province, School of Public Health, Hengyang Medical School, University of South China, Hengyang 421001, China

^e School of Chemical and Materials Engineering, National University of Sciences and Technology (NUST), Islamabad 44000, Pakistan

ARTICLE INFO

Keywords:

MXene
Molybdenum Disulphide
Water treatment
Adsorption
Hexavalent Chromium removal

ABSTRACT

Chromium is a carcinogenic heavy metal that accumulates in plant and animal bodies. New materials for efficient removal of chromium from water bodies are in high demand. MXene was synthesized from MAX phase by using ammonium fluoride as an etching agent while molybdenum disulphide was synthesized by hydrothermal method. The pseudo-second order kinetic model described the adsorption of hexavalent chromium on MXene and molybdenum disulphide whereas the Freundlich Isotherm model best fitted for MXene, and Langmuir Isotherm model was more suitable in case of molybdenum disulphide. The adsorption capacity obtained by MXene for hexavalent chromium was 59.8 mg/g (At Dosage = 1 g/L, T = 298 K, Time = 9 h, pH = 2, C₀ = 30 mg/L) and 113.7 mg/g in case of molybdenum disulphide (At Dosage = 0.5 g/L, T = 298 K, Time = 1.5 h, pH = 2, C₀ = 30 mg/L). Thermodynamic investigations showed that the process was endothermic and spontaneous. The coexisting ions showed a decrease in removal percentage up to 70 % and 79 % in case of MXene and molybdenum disulphide, respectively, after fifth cycle. It can be inferred that these developed materials have the advantages of simplicity for reducing heavy metal pollution.

1. Introduction

The distribution of heavy metals due to industrial developments has resulted in water adulteration worldwide in the past few years. Heavy metal pollution is contributed by multiple heavy metal ions such as Zn (II), Hg(II), Pb(II), Cu(II), Cd(II) and Cr(VI). Among all these pollutants, Cr(VI) is a common pollutant which exists in different ionic forms in contaminated water [1]. The increased concentrations of chromium has very bad effect on both humans and other organisms after mercury, lead and cadmium [2]. The sources of chromium can both be natural and artificial due to human anthropogenic stresses [3]. Increase of Cr (VI) in the environment also occurs from the natural processes in groundwater mainly due to the interaction of existing water with ultramafic rocks [4]. Other sources of Cr(VI) in ground water originate

from geogenic sources. In these processes, natural leaching of chromium occurs into water from the surrounding rocks having higher concentrations of chromium [5]. Additionally, Cr(VI) is formed naturally by manganese catalysis. Cr(VI) in water treatment can also result from oxidative processes such as ozonation and chlorination [6]. Numerous industries, including the tanning of leather, metal plating, electroplating, military, pigment, and refractory industries, use chromium extensively. Wastewater generated from industrial processes is a primary source of release of Cr(VI) to water bodies mainly from cement industries, paint industries, wood preservation, manufacturing of stainless steel, electroplating and metallurgical processes [7]. Industrial effluents release chromium oxide in its +2 to +6 chemical states into aquifers and streams, among other receiving habitats. The two most recurrent forms of chromium are trivalent Cr(III) and Cr(VI) Cr(VI)

Abbreviations: MoS₂, Molybdenum Disulphide; Cr III, Trivalent Chromium; Cr VI, Hexavalent Chromium; WHO, World Health Organization; EPA, Environmental Protection Agency; USEPA, United States Environmental Protection Agency; EU, European Union; XRD, X-ray Diffraction; FTIR, Fourier Transform Infrared Spectroscopy; SEM, Scanning Electron Microscopy; BET, Brunauer Emmett Teller; EDS, Energy Dispersive X-ray Spectroscopy

* Corresponding authors.

E-mail addresses: waheed.miran@scme.nust.edu.pk (W. Miran), musharib@iese.nust.edu.pk (M. Khan).

<https://doi.org/10.1016/j.dwt.2024.100693>

Received 22 May 2024; Received in revised form 2 August 2024; Accepted 4 August 2024

1944-3986/© 2024 The Author(s). Published by Elsevier Inc. This is an open access article under the CC BY license (<http://creativecommons.org/licenses/by/4.0/>).

owing to their malignancy and substantial impacts to the environment. The poisonousness of Cr(VI) is noticeably higher than Cr(III) [7]. The toxicity of Cr(VI) in terms of carcinogenicity and mutagenicity is 500 times greater than Cr(III) [8]. Compared to the Cr(III) form, the extremely poisonous, soluble, and mobile Cr(VI) form has more detrimental effects on both people and animals [9].

Permissible limits for the targeted pollutant by the World Health Organization are regulated to be 0.05 mg/L [10]. According to USEPA, permissible concentration of Cr(VI) in water is 0.1 mg/L. These strategic standards impose the restrictions of excessive discharge of Cr(VI) in drinking water [7]. Directive drinking water of European Union recommends Cr(VI) level up to 25 µg/L [6]. Furthermore, in future, strict regulations are expected for Cr(VI) concentrations due to its potential health impacts.

Cr(VI) is known to be carcinogenic and is the cause of numerous diseases which mainly includes lung cancer, damage to kidney and liver, gastrointestinal problems, skin and nasal irritation, eardrum damage, [11] dermatitis, respiratory disorders, and eye infections. According to the international literature, Cr(VI) is the leading cause of dysfunction of digestive system, immune system, urinary system, respiratory and reproductive systems as well [12]. Cr(VI) is also referred as Group A carcinogen [13]. The effect of chromium on human body is regulated by multiple factors such as the duration of exposure, dosage of chromium intake, form of chromium which is also dependent on the route of its intake such as through food, water, inhalation or with skin contact. Cr(VI) exposure over an extended period of time may be harmful to health and is influenced by a number of variables, including body weight, age, and gender [4]. Cr(VI) is classified in different categories depending on the time and duration of its exposure. The exposure is considered acute if exposed to Cr(VI) for 14 days. The exposure is referred as intermediate if it lasts between 75 to 364 days and it will be chronic exposure if it extends to 365 days according to the literature reports [12,14].

Many techniques have been used to remove heavy metals from wastewater and water. These methodologies primarily include membrane separation [15], degradation [16], flocculation [17], photocatalysis [18], co-precipitation [19], electrolysis [20], chemical reduction [21], ion exchange [22], reverse osmosis [23], and other biological methods [24]. Currently adsorption is a growing substitute technique for the remediation of Cr(VI) owing to its simplicity, reusability, economy, effortless operation, maintenance, and improved effectiveness. The creation of a novel adsorbent with features and attributes that suggest a high adsorption capacity for metal ions is required, given the benefits of adsorption. A number of adsorbents have been used to trap Cr(VI) such as activated carbon [25], zeolites, layered double hydroxides [26], metal oxides, graphene oxides [27], polymers [28], carbon nanotubes [29], metal organic framework [30] and nanoscale zero valent iron [31]. However, many of the materials have shown unsatisfactory results due to low efficiency, weak adsorption and resulting secondary pollution. It is mandatory to explore new materials for the treatment of chromium pollution with improved stability.

MXene and MoS₂ are regarded as two popular two-dimensional nanomaterials in water treatment [32]. They have been investigated extensively for adsorption of environmental pollutants with numerous modifications. MXenes are a class of two-dimensional transition metal nitrides, carbides and carbonitrides with intriguing chemical, mechanical, electrical, and magnetic properties [33]. The chemical formula of two dimensional MXenes nanomaterials is M_{n+1}X_nT_x where n can be any number between 1 and 3. M in the formula represents early transition metals of periodic table such as Sc, W, Ti, Cr, Mo Ta, Zr, W, Nb, Hf, V or Y), X represents nitrogen or carbon and T represents the surface terminating group such as hydroxyl (-OH), Chlorine (-Cl), Fluorine (-F) or Oxygen (=O) and x stands for the surface functionalities [34,35]. Typically, MXenes are prepared from MAX phases by etching the Al atoms in layered hexagonal ternary carbide Ti₃AlC₂ in targeted manner. On the other hand, MoS₂ is an inorganic compound which is

formed by the combination of one molybdenum atom and two sulfur atoms, and it is categorized as transition metal dichalcogenides [36]. MoS₂ nanosheets can be synthesized by numerous techniques. Some of the methods mentioned in the literature are chemical exfoliation [37], mechanical exfoliation [38], electrochemical exfoliation [39], liquid exfoliation [40], chemical vapor deposition [41] and hydrothermal synthesis [42].

The purpose of this study is to compare the potential of two-dimensional nanomaterials in the removal of Cr(VI) under optimum working conditions. Materials were synthesized and tested through different characterization methods. XRD, FTIR, SEM, EDS and BET surface area analysis were performed to depict the crystallinity of the adsorbents, investigation of the functional groups, morphology of structures and their elemental composition, and to check the surface area of MXene and MoS₂, respectively. Adsorption studies were conducted to investigate the use of efficient two-dimensional nanomaterials for Cr(VI) removal. Furthermore, the adsorption capacities of MXene and MoS₂ were compared for Cr(VI) adsorption.

2. Materials and methods

2.1. Chemical reagents

Ternary carbide MAX powder (Ti₃AlC₂) was kindly provided by Dr. Asif Shahzad (Uppsala University, Sweden). Hydrochloric acid (49 %), Ammonium Fluoride, Polyvinyl Pyrrolidone (PVP), NaOH, K₂Cr₂O₇, Syringe Filters, Acetone, Diphenyl Carbazide (DPC), Orthophosphoric Acid, Thiourea, Ammonium Heptamolybdate, Acetic Acid, Tetrahydrate, Ethanol was purchased from Sigma Aldrich. All necessary chemicals were utilized without any additional purification. For experiments and washing, deionized water was used.

2.2. Synthesis of MoS₂

For the preparation of MoS₂, 5 mmol of ammonium heptamolybdate (NH₄)₆Mo₇O₂₄ was immersed in 25 mL of water at room temperature. 0.15 g of polyvinyl pyrrolidone (PVP) K30 (C₆H₉NO)_n was added to the mixture at low temperature using an ice bath. The solution was further sonicated for 60 min. After sonication, 10 mmol of thiourea (CH₄N₂S) was added to the solution after sonication and continuously stirred for 30 min. Further autoclave 1.5 mL of acetic acid (CH₃COOH) was added to the solution before transferring the solution to autoclave. The autoclave was kept in a 180 °C oven for a whole day. After the autoclave was cooled to room temperature, methanol and water were used to filter the black particles multiple times. The mixture was then dried for 24 h at 80 °C.

2.3. Synthesis of MXene

MXene was synthesized by the process of etching. This process used ammonium fluoride (NH₄F) as an etching agent to produce MXene. At room temperature (298 K), 0.5 g of MAX phase powder (Ti₃AlC₂) that had been sieved with 200 screen was slowly immersed in 100 mL of 1 M NH₄F. The mixture was then agitated for a whole day. After centrifuging the sedimented solids for 15 min at 6000 rpm, the pollutants were entirely removed using deionized water, and the dispersion's pH was stabilized at around 7. In order to create the synthesized Ti₃C₂T_x MXene, the filtrate was dried for 24 h at 60 °C in a vacuum oven and then stored for later use.

2.4. Preparation of Cr(VI) stock solution

Chromium stock solution was prepared using potassium dichromate (K₂Cr₂O₇). In a 1000 mL volumetric flask, 2.83 g of K₂Cr₂O₇ (99 % purity) was dissolved into 1000 mL of deionized water to freshly prepare 1000 mg/L Cr(VI) stock solution. After giving the mixture a good shake, it was put to use in other experiments.

2.5. Batch adsorption measurements

In the adsorption experiments for the removal of chromium, batch technique was applied. In a typical procedure, 5 mg of MoS₂ and 10 mg of MXene was immersed in 10 mL of chromium solution with concentration varying from 20 mg/L to 120 mg/L, respectively, and shaken at 120 rpm at 298 K. After adsorption, solid residue was separated using 0.2 µm syringe filters. The supernatant was further used for measuring adsorbent's removal efficiency. Cr(VI) concentration was measured using the standard curve shown in (Fig. S1) using UV vis spectrophotometer by diphenyl carbazide method at a wavelength of 540 nm [43]. After adsorption, adsorbents were washed with deionized water and desorption reagent (0.1 M NaOH) for recycling experiments. To check the effect of pH, pH tests were conducted by adjusting pH from 2 to 8 using 0.1 M HCl and 0.1 M NaOH solutions. Kinetics studies were conducted at a fixed concentration of 30 mg/L at 298 K for designated time. Also, the ionic strength of different cations and anions was applied to investigate the effect of competitive ions on Cr(VI) removal. All the kinetics and isotherm studies were conducted at 3 different temperatures (298 K, 308 K, and 318 K) for thermodynamic studies. At last, the removal efficiency and adsorption capacities were measured for chromium by MoS₂ and MXene, respectively, using the following equations.

2.5.1. Adsorption capacity and removal percentage

The adsorption capacity and removal percentage were calculated by the relations as follows:

$$Q_e = (C_o - C_e) \times V/m \quad (1)$$

$$R = (C_o - C_e) / C_o \times 100\% \quad (2)$$

where C_o is the pollutant's Cr(VI) initial concentration, C_e is the final concentration, V is the working volume and m is the mass of adsorbent used in the experiment.

2.6. Material characterization of MoS₂ and MXene

The morphology of the synthesized adsorbents was analyzed by Scanning Electron Microscopy (SEM) (JSM6940LA Analytical Low Vacuum SEM). The functional groups on the adsorbents were characterized through Fourier-transform infrared (FTIR) spectroscopy (PerkinEimer Spectrum 100 FTIR Spectrophotometer) in the range of 400 to 4000 cm⁻¹. The crystalline nature of the adsorbents was studied through acquiring their powder X-ray diffractograms using an X-ray diffraction (XRD) spectrometer (BRUKER 2D Phaser) in the 2θ range from 0° to 80°. The specific surface area, pore volume, and pore size distribution of the samples (degassed at 180 °C for 24 h) were determined by the Brunauer–Emmett–Teller (BET) method using a surface area analyzer (Gemini VII 2390 t, Micromeritics). The zeta potential measurements were conducted using a zeta potential analyzer (Wallis Zeta Potential Analyzer, Cordouan Technologies).

3. Results and discussion

3.1. Material characteristics of the synthesized adsorbents

3.1.1. SEM analysis

Morphologies of MoS₂ and MXene were analyzed by Scanning Electron Microscope. SEM analysis of the MXene showed thin layered surface arrangement (Fig. 1A) representing lamella like structure (Fig. 1B). The synthesized MXene exhibits accordion-like structures that indicate layer breaking, in contrast to Ti₃AlC₂ which exhibits a brick like structure with compacted layers connected with strong metallic bonds of Titanium and Aluminium [44]. Figs. 1C and 1D show the flower-like structure of MoS₂ at a scale of 2 µm and 1 µm, respectively. The interconnected spherical MoS₂ particles indicate a porous material

structure. This porosity of clustered nanoparticles is often associated with better adsorption performance [45]. Cr(VI) The results reported in this research for both the nano materials are mostly similar to those documented in the literature [44,45].

3.1.2. EDS analysis

After etching with NH₄F, EDS examination of MXene reveals that Al is significantly reduced and the layers are separated. The removal of Al verifies the formation of MXene and presence of surface terminations of functional groups such as O, and fluorine groups (Fig. 1E). In the case of MoS₂ (Fig. 1F), it can be seen that the sample majorly comprises of Mo and S. The elemental composition determined from EDS for MoS₂ constitutes S (58.4%), O (2.6%), C (2.8%), and S (36.2%), while for MXene, it includes Ti (62.6%), C (20.8%), O (11.6%), and F (2.9%).

3.1.3. XRD analysis

XRD analysis of MXene and MoS₂ was performed to assess the crystalline structures and interlayer spacing of the particles. A strong and clear peak of Ti₃AlC₂ is visible at 2θ = 39° corresponding to (104) in Ti₃AlC₂. Other peaks of Ti₃AlC₂ are shown at 9.33°, 19.25°, 33.82°, 41.61° corresponding to (002), (004), (003) and (105), respectively. As the MXene was etched by NH₄F, the peak at (104) disappeared and smaller peak at 27.3° was observed corresponding to (008) diffraction. An unspecific TiC impurity peak was seen at 38° as shown in Fig. 1G. XRD results of MXene are consistent with standard pattern JCPDS no: 52–0875. Moreover, after etching, the peak of MXene is moved towards the smaller angle and gets broaden which confirms the enlarged interlayer spacing in MXene [44]. From the XRD results, it can be concluded that etching of Ti₃AlC₂ with NH₄F resulted in the weakening of Al-Ti metal bond and Al element was taken out from MAX phase [46]. XRD pattern of MoS₂ shows peaks at different diffraction angles of 14.2°, 33.4°, 39.6°, 49.36°, and 58.86°, respectively corresponding to (002), (100), (103), (105), and (110) characteristic peaks of MoS₂ (Fig. 1H) [47]. Pattern of MoS₂ are in good agreement to the standard XRD pattern JCPDS no: 37–1492 [48]. The creation of many layers along the (002) direction is shown by the peak of (002) [47].

While other peaks at 33.4°, 39.6°, 49.36°, and 58.86° are created due to interlayer interactions and the peak at 14.2° is formed due to the scattering of Mo-Mo atomic layers in the MoS₂ interlayer [49]. The XRD results confirm the successful synthesis of crystalline MXene and MoS₂ as documented in the literature.

3.1.4. FTIR and BET analysis

FTIR is a characterization technique for describing surface structure and associated functional groups of any sample. Fig. 2A shows the FTIR spectrum of MXene before adsorption in which a clear peak of OH⁻ group appears at 3435 cm⁻¹ confirming the presence of hydroxyl functional groups on the surface of synthesized MXene. Other typical peaks of MXenes appeared at 1637 cm⁻¹, 1289 cm⁻¹, 869 cm⁻¹, and 544 cm⁻¹ representing H-OH, C-H, C=O, and Ti-O, respectively. After Cr(VI) adsorption, the intensities of functional groups on the surface of MXenes were weakened. The intensity of -OH group decreased, and the peak shifted from 3435 cm⁻¹ to 3444 cm⁻¹ which shows the interaction of OH group and Cr during adsorption [50]. The peak at 1628 cm⁻¹ is attributed to H-OH stretching vibrations of MXenes [34]. Similarly, the shifts in other peaks with reduced intensity after the adsorption confirm further that Cr(VI) is successfully adsorbed on the surface of MXenes. Unlike MXenes, the spectrum of MoS₂ before adsorption (Fig. 2B) showed a peak at 596 which corresponds with Mo-S stretching vibrations [51]. Peaks at 1055 cm⁻¹ and 1215 cm⁻¹ were associated with C-N-H stretching vibrations [49] which merged and shifted to 1047 cm⁻¹ after adsorption. Peak at 1645 cm⁻¹ shows the bending vibrations of hydroxyl group (-OH) [49]. Peak at 3474 cm⁻¹ before adsorption is attributed to stretching vibrations of hydroxyl group which shifted to 3419 cm⁻¹ with reduced intensity after adsorption [52].

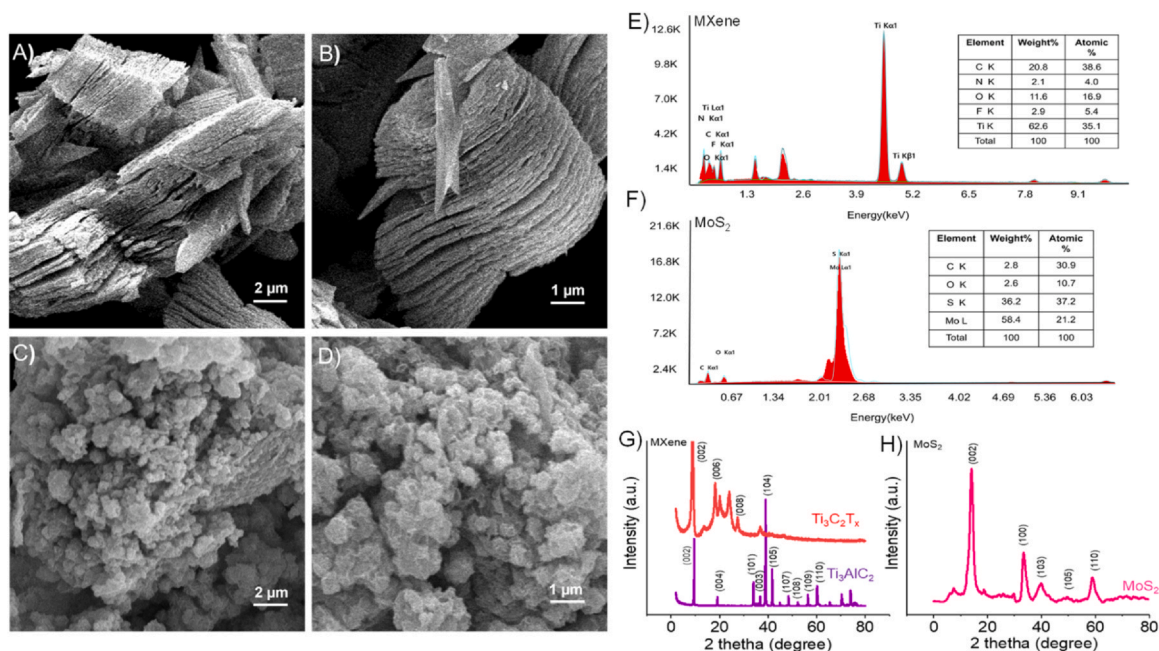


Fig. 1. SEM micrographs of MXene (A-B) and MoS₂ (C-D) at different magnifications. EDS analysis of MXene (E) and MoS₂ (F). XRD analysis of MXene (G) and MoS₂ (H).

The shifts occurring in the FTIR spectrum of MoS₂ after adsorption indicate that chemical interactions occur between the MoS₂ and Cr(VI) [53]. The BET analysis showed that the surface area for MXene and MoS₂ was 5.3 and 4.7 m²/g, respectively.

3.2. Effect of operational parameters on adsorption of Cr(VI) onto MXene and MoS₂

Numerous batch experiments were performed to examine the impact of various parameters on the adsorption of chromium onto MXene nanosheets and pure MoS₂.

3.2.1. Effect of solution pH on adsorption

The pH of solution is a very essential parameter in determining the speciation of chromium in water as it controls the ionic forms and valence states of heavy metals. The effect of pH ranging from pH (2 to 8) on both MXene and MoS₂ is shown in Figs. 3A and 3B, respectively. It can be seen that the maximum removal of MXene and MoS₂ is shown at pH 2 whereas the increase in pH of solution decreases the adsorption capacity which confirms that the pH influences the removal capacity of

adsorbent. Similarly, for MoS₂, the removal of Cr(VI) shows strong dependency on pH as maximum removal of Cr(VI) is found at pH 2 after 90 min. When the pH of solution was increased to pH 8, the adsorption capacity is reduced to 26.9 mg/g. Chromium dissociates into different oxyanions in water.



The existence of different ions for Cr(VI) is regulated by pH. Within the pH range of 2–6, the dominant species of chromium are Cr₂O₇²⁻ and HCrO₄⁻ and at pH > 6, CrO₄²⁻ species become dominant in water [52]. H₂CrO₄ dominates at pH < 1 [54]. The zeta potential values are also maximum at pH 2 for both MXene and MoS₂ which indicates the higher percentage of HCrO₄⁻ over Cr₂O₇²⁻ at lower pH value [55]. The change in zeta potential values of MXene and MoS₂ at different pH values is shown in Fig. S2A and S2B, respectively. MXenes show good chromium removal in acidic pH due to the protonation of the surface of MXene nanosheets [34]. In the case of MoS₂, the addition of PVP during

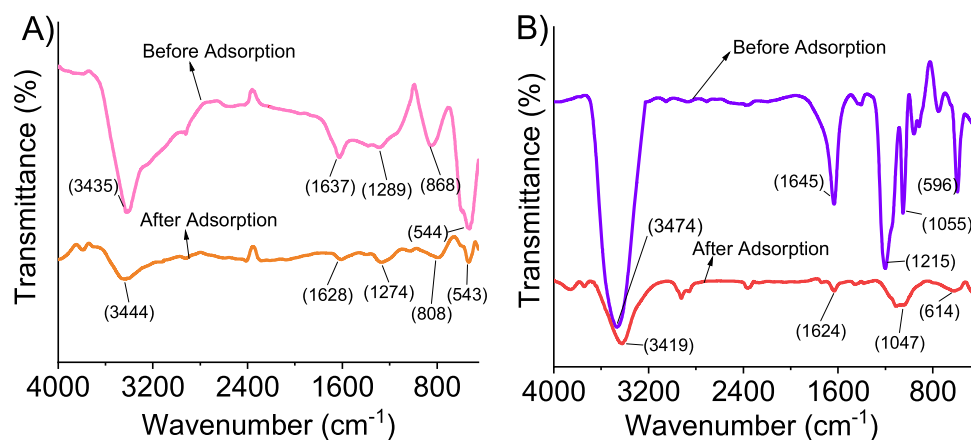


Fig. 2. FTIR analysis of (A) MXene and (B) MoS₂ before and after Cr(VI) adsorption.

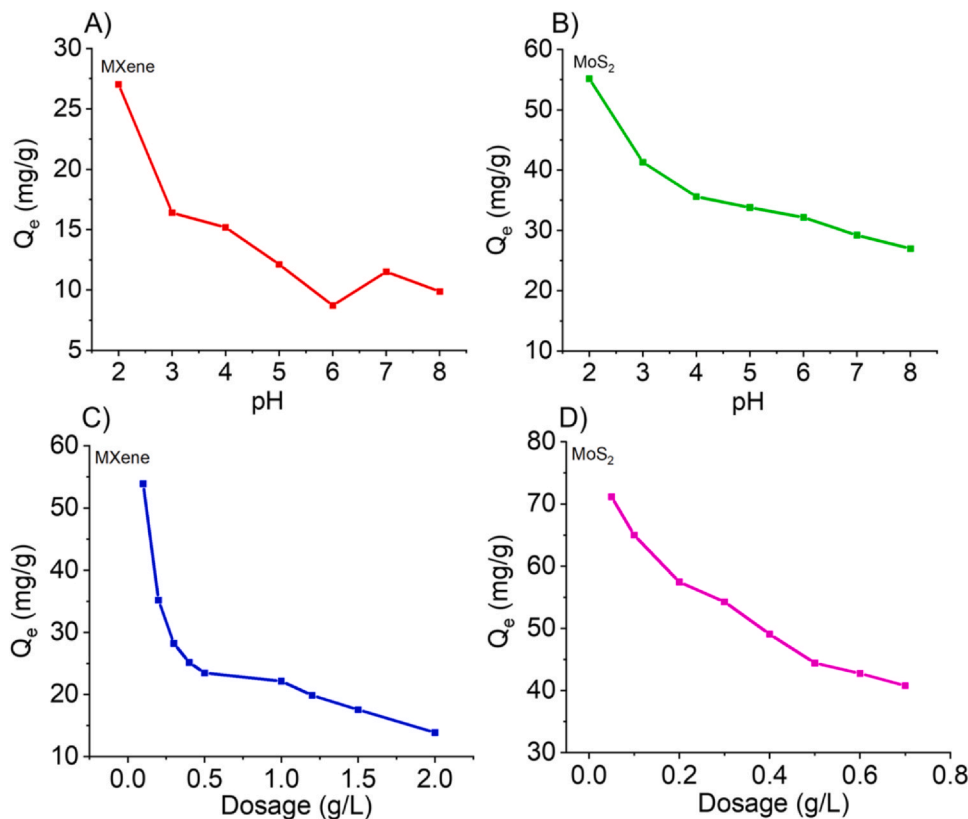


Fig. 3. Effect of pH on adsorption capacity (A) MXene Co = 30 mg/L, T = 298 K, Time = 9 h, Dosage = 1 g/L and (B) MoS₂ Co = 30 mg/L, T = 298 K, Time = 1.5 h, Dosage = 0.5 g/L. Dosage effect on removal percentage and adsorption capacity. (C) MXene Co = 30 mg/L, T = 298 K, Time = 9 h, pH = 2 and (D) MoS₂ Co = 30 mg/L, T = 298 K, Time = 1.5 h, pH = 2).

synthesis process induces positive charge on its surface [56]. This makes it highly protonated due to the strong electrostatic force of attraction between adsorbate and adsorbent in aqueous media. Acidic pH is more favorable in the removal of chromium [57]. Based on these results, pH 2 was taken as the optimum pH for both adsorbents which was further applied in the following studies.

3.2.2. Effect of adsorbent’s dosage on adsorption

At MXene (Fig. 3C) and MoS₂ (Fig. 3D), the impact of adsorbent dosage was examined using dosages of materials ranging from 0.1 to 2 g/L and 0.1 to 0.7 g/L, respectively, while maintaining concentration of Cr(VI) at 30 mg/L, solution temperatures of 298 K for both MXene and MoS₂ and pH = 2. In the case of MXene (Fig. 3C), the adsorption capacity decreased sharply from 53.8 mg/g to 19.8 mg/g with an increase of dosage from 0.1 g/L to 1.2 g/L. The adsorption rate was maximum with further increase in dosage up to 2 g/L indicating almost complete removal of Cr(VI). Similarly, for MoS₂, the adsorption capacity of chromium was decreased from 71.1 mg/g to 42.7 mg/g with adsorbent dosage varying from 0.05 g/L to 0.6 g/L which was further decreased to 40.7 mg/g at 0.7 g/L MoS₂. The optimum dosage value chosen for MXene and MoS₂ was 1 g/L and 0.5 g/L, respectively, for further experimentation.

3.2.3. Effect of time on adsorption

This study aims to analyze the effect of time on the adsorption of MXene and MoS₂ and the outcomes are displayed in Figs. 4A and 4B, respectively. Adsorption of Cr(VI) was performed keeping dosage of MXene 1 g/L and MoS₂ dosage of 0.5 g/L, an initial chromium concentration of 30 mg/L, temperature of 298 K, 308 K and 318 K, and pH value of 2. Q_e achieved after 9 h was 24.3 mg/g for MXene and Q_e achieved for MoS₂ was 47.1 mg/g after 90 min. Chromium removal was faster by MoS₂ as compared to MXene. The enhanced chromium adsorption of MoS₂ is due to the unique structural arrangement of MoS₂ with enlarged interlayer spacing. The defects in the structure acted as

permeable channels in the diffusion of ions in the bulk of MoS₂. Upon saturation of MXene and MoS₂, the uptake of Cr(VI) decreases and finally equilibrium is achieved.

3.3. Kinetics of Cr(VI) adsorption onto MXene and MoS₂

Reaction time determines the efficiency of the absorbent in its practical application. Therefore, two dimensional nanomaterials MXene and MoS₂ were selected to check their performance for Cr(VI) removal. Compared to MoS₂, longer time was taken by MXene to achieve adsorption equilibrium with lower adsorption capacity. In order to research both material’s adsorption rate and their role in potential rate limiting steps, linear and nonlinear kinetics of different models were applied on both materials. The following equations were used to compute the kinetics curves for Cr(VI) adsorption at three different temperature values on MXene and MoS₂ for the pseudo first order, pseudo second order, Elovich model and Intraparticle Diffusion Model.

3.3.1. Pseudo-first order

$$Q_t = Q_e(1-\exp(-k_1t)) \dots \dots \dots \text{Non-Linear} \tag{6}$$

$$\log(Q_e-Q_t) = (\log(Q_e)-k_1t / 2.303) \dots \dots \dots \text{Linear} \tag{7}$$

where k_1 denotes pseudo first order rate constant, Q_e is the adsorption capacity (mg/g) at equilibrium and Q_t is the adsorption capacity at time t, (min) for MoS₂ and (hour) for MXene.

3.3.2. Pseudo-second order

$$Q_t = Q_e^2 k_2t / Q_e k_2t + 1 \dots \dots \dots \text{Non-Linear} \tag{8}$$

$$t / Q_t = (1 / k_2Q_e^2 + t / Q_e) \dots \dots \dots \text{Linear} \tag{9}$$

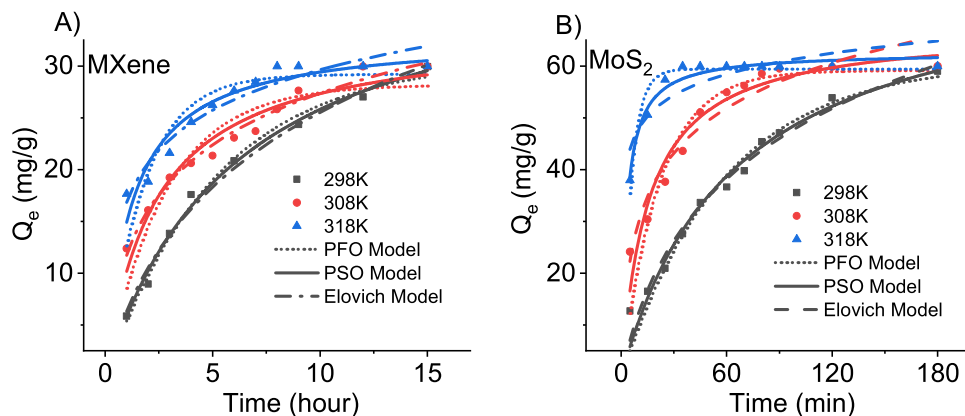


Fig. 4. Effect of time on Cr(VI) adsorption and nonlinear kinetics of different models (PFO, PSO, Elovich) for Cr(VI) adsorption (A) MXene Co = 30 mg/L, T = 298 K, Dosage = 1 g/L, pH = 2) and (B) MoS₂ Co = 30 mg/L, T = 298 K, pH = 2, Dosage = 0.5 g/L).

Where k_2 denotes pseudo second order rate constant, The adsorption capacity (mg/g) at equilibrium is denoted by Q_e , while the adsorption capacity at time t is represented by Q_t , (min) for MoS₂ and (hour) for MXene.

3.3.3. Elovich model

$$Q_t = (1/\beta)\ln(1 + \alpha\beta t) \dots\dots\dots\text{Non-Linear} \quad (10)$$

$$Q_t = \beta\ln(t) + \beta\ln(\alpha\beta) \dots\dots\dots\text{Linear} \quad (11)$$

where while the adsorption capacity at time t is represented by Q_t , (min) for MoS₂ and (hour) for MXene. α represents the principal adsorption rate. The desorption parameter, or β , is used to describe the degree of chemisorption and activation energy.

3.3.4. Intraparticle diffusion

$$Q_t = K_{ip} t^{(1/2)} + C \quad (12)$$

The fitting curves for linear kinetics are shown in Fig. 5 for MXene (A-D) and MoS₂ (E-H) whereas the nonlinear kinetics curves are

displayed in Fig. 4A and Fig. 4B. All the chi square values and kinetic parameters of MXene and MoS₂ adsorbents are shown in Table S1 and Table S2. From the tables, it can be clearly observed that the linearized and non-linearized pseudo second order shows higher values of correlation coefficients of R^2 for MXene and MoS₂, respectively than pseudo first order and Elovich model. The pseudo-second order Q_e values that are computed also fit well with the experimentally determined Q_e values. Additionally, Q_e calculated by the non-linearized equation is well suited to $Q_{e,exp}$ than linearized equation which suggests that experimental data is more coherent to non-linearized pseudo second order kinetic model than linearized one. Additionally, the pseudo second order model's computed values of X^2 are lower than those of the pseudo first order model, confirming the suitability of the pseudo second order model for the adsorption kinetics process and suggesting that chemisorption for both MXene and MoS₂ is a part of the adsorption process.

Additionally, pseudo first order, pseudo second order and Elovich model do not explain the diffusion mechanism of Cr(VI) removal. As a result, Weber and Morris' inter particle diffusion model was applied at 298 K, 308 K, and 318 K to study the diffusion process and rate-limiting steps of the adsorption process on MXene and MoS₂ as shown in Fig. 5D and Fig. 5H, respectively. Q_t is the Cr(VI) adsorbed quantity at time t (mg/g), k_{ip} stands for the rate constant of the model, (g/mg/time), t is

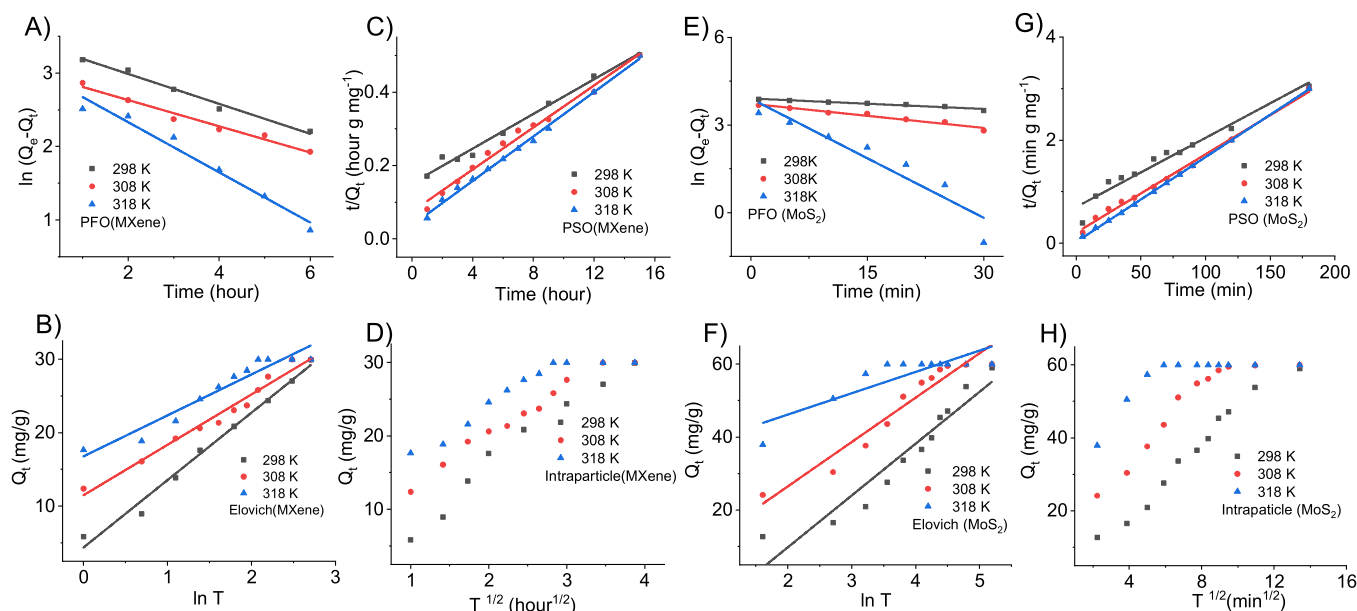


Fig. 5. Linear kinetics of different models (A) PFO, (B) PSO, (C) Elovich, (D) Intraparticle Diffusion for Cr(VI) adsorption by MXene at T = 298 K, 308 K, 318 K. Linear kinetics of different models (A) PFO, (B) PSO, (C) Elovich, (D) Intraparticle Diffusion for Cr(VI) adsorption by MoS₂ at T = 298 K, 308 K, 318 K.

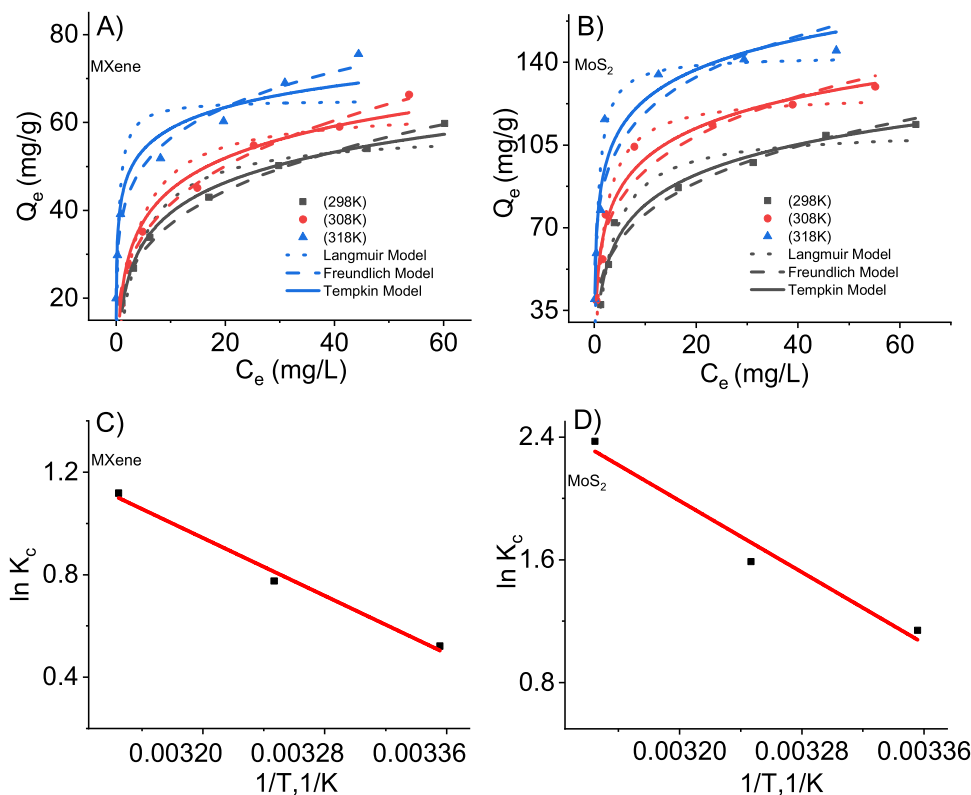


Fig. 6. Fit of data to nonlinear isotherms of Langmuir, Freundlich and Temkin Model (A) MXene and (B) MoS₂. Thermodynamic parameters plot for Cr(VI) adsorption by MXene (C) (Dosage = 1 g/L, Co = 30 mg/L, Time = 9 h, pH = 2) and MoS₂ (D) (Dosage = 1 g/L, Co = 30 mg/L, Time = 1.5 h, pH = 2).

for the contact time which is (min) for MoS₂ and (hour) for MXene and C denotes the intercept written as (mg/g). Different intraparticle diffusion rate constants such as k_{ip} and C were calculated at three temperature values using slope and intercept values of the graphs and the results are shown in Table S3. Based on the data, it can be inferred that the boundary layer's influence on the surfaces of MXene and MoS₂ is what caused the first adsorption. Adsorption is redirected towards porous diffusion on the interior structures of MXene and MoS₂ as the active sites on their surface decrease. At the end stages of adsorption curve, adsorption reaches equilibrium as shown in Fig. 5D and Fig. 5H for MXene and MoS₂, respectively. As a result, the adsorption process involves two different types of diffusion mechanisms i.e. adsorption on surface and internal diffusion. [58].

3.4. Cr (VI) concentration's impact on adsorption

To determine the ideal circumstances for the removal of Cr(VI), a comparison analysis was carried out for both MXene and MoS₂. Using seven Cr(VI) concentrations ranging from 20 mg/L to 120 mg/L, the effects of pollutant concentration on the adsorption capabilities of both adsorbents were examined and the findings are shown in Fig. 6A of MXene and Fig. 6B of MoS₂. The oversupply of vacant adsorption sites on the surface of adsorbents at lower concentrations may be the cause of the quick increase in the adsorption capacities at the beginning stages, as seen in the figures showing how the adsorption capacities of MXene and MoS₂ increased with an increase in Cr(VI) concentration. However, the number of adsorption sites on the adsorbent's surface decreased as Cr(VI) concentration increased, acting as a limiting step for Cr(VI) adsorption [59,60].

3.5. Adsorption isotherm study

To study the interaction of adsorbate on the surface of adsorbent, isotherm models are studied. In this study, adsorption isotherm was

fitted using Langmuir, Freundlich and Temkin isotherms models at three different temperatures 298 K, 308 K and 318 K as shown in Figs. 6A and 6B. To find the maximum adsorption capacities and gain a better understanding of the adsorption process, experimental data was simulated using Langmuir, Freundlich, and Temkin isotherms. The following are the linearized and non-linearized equations for each of the three models that were used.

The monosaturated layer of adsorbate on the surface of the adsorbent is responsible for the highest adsorption, according to the Langmuir Isotherm Model. There is less adsorbate transmigration, and the adsorption energy is constant. As the distance from the adsorption surface rises, the intermolecular interactions become weaker and the energy of the active sites remains constant [61].

Equations of Langmuir model are as follows.

$$Q_e = (Q_m * K_L * C_e) / (1 + K_L * C_e) \dots\dots\dots \text{(Non-Linear)} \quad (13)$$

where Q_m is the maximum adsorption capacity (mg/g).

K_L is the Langmuir constant (L/mg).

$$C_e / Q_e = C_e / Q_m + 1 / (Q_m * K_L) \dots\dots\dots \text{(Linear)} \quad (14)$$

Q_m is determined by the slope and K_L is measured from the interaction of fitted line on abscissa (C_e) and ordinate (C_e / Q_e).

Langmuir isotherm (R_L) is also known as balance parameter as it is a dimensionless constant having formula as follows.

$$R_L = 1 / (1 + K_L * C_i) \quad (15)$$

where R_L is dimensionless constant, C_i is the initial concentration of Cr (VI) pollutant.

The adsorbent's heterogeneous surface is connected to the Freundlich isotherm model, which also explains the exponential behavior of the active sites and their binding energies [62]. Equations of Freundlich model are as follows.

$$Q_e = K_F + C_e^n \dots\dots\dots \text{(Non-Linear)} \quad (16)$$

Table 1

Thermodynamics parameters for Cr(VI) adsorption by MXene (Dosage = 1 g/L, $C_o = 30$ mg/L, Time = 9 h, pH = 2) and MoS₂ (Dosage = 1 g/L, $C_o = 30$ mg/L, Time = 1.5 h, pH = 2).

Adsorbent	T (K)	Thermodynamic Parameters			
		ΔG°	ΔH°	ΔS°	R^2
		(kJ/mol)	(kJ/mol)	(kJ/mol/K)	
MXene	298	-1.291	23.469	0.069	0.978
	308	-1.985			
	318	-2.956			
MoS ₂	298	-2.825	48.322	0.171	0.939
	308	-4.066			
	318	-6.269			

K_F is the Freundlich constant (mg/g), and n represents Freundlich exponent related to the intensity of adsorption. n is dimensionless. Linearized equation of the Freundlich model is as follows.

$$\log Q_e = (1/n) \log C_e + \log K_F \dots\dots\dots \text{(Linear)} \quad (17)$$

n is determined by the slope and K_F is determined from intercept of fitted graphical line on abscissa ($\ln C_e$) and ordinate ($\ln Q_e$).

The value of $1/n$ range from 0 to 1 and depicts the degree of non-linearity between adsorption and concentration of solution. Value of $(1/n) = 1$ shows linear adsorption. Lower values of n corresponds to the presence of abundant high energy active sites whereas higher values of n shows that the surface is a bit uniform in structure [63].

Temkin isotherm model describes the interactions between the adsorbate and species. Equations of Temkin model are as follows.

$$Q_e = (RT/b) \ln(K_T * C_e) \dots\dots\dots \text{(Non-Linear)} \quad (18)$$

where.

$$(RT/b) = B \quad (19)$$

b represents Temkin constant. K_T is for Bound Equilibrium constant (L/g) and B is referred as heat of adsorption with units J/mol. Linearized equation of the Temkin model is as follows.

$$Q_e = B \ln C_e + B \ln K_T \dots\dots\dots \text{(Linear)} \quad (20)$$

Plotting Q_e on the ordinate and $\ln C_e$ on the abscissa allows one to compute B and K_T from the slope and intersections of the lines fitted. [63].

The fitting plots of linear Langmuir, Freundlich and Temkin models for the removal of Cr(VI) are shown in Fig. S3(A-C) and S4(A-C) for MXene and MoS₂, respectively. Also, isotherm parameters and chi square values calculated from the experimental data are shown in Table S4.

From table S4 it can be concluded that for Cr(VI) adsorption at MXene nanosheets, Freundlich linear and nonlinear isotherms had higher R^2 values as compared to linear and nonlinear Langmuir and Temkin isotherm models. In addition to that, X^2 values of Freundlich isotherm model are lower than Langmuir isotherm model. Compared to the linear and nonlinear Freundlich and Temkin isotherm model, the linear and nonlinear Langmuir isotherm model in the case of MoS₂ showed higher R^2 values. Furthermore, the Freundlich isotherm model has higher X^2 values than the Langmuir isotherm model. Freundlich and Langmuir isotherm models appear to fit MXene and MoS₂ the best, according to higher R^2 and lower X^2 values, respectively. The maximum adsorption capacities achieved in case of both adsorbents were close to experimental values at different temperatures of 298 K, 308 K and 318 K. The fitting of Freundlich model in case of MXene suggests that process of Cr(VI) adsorption at MXene nanosheets was heterogenous

adsorption and the highest adsorption capacities achieved at 298 K, 308 K and 318 K were 59.8 mg/g, 66.3 mg/g, and 75.5 mg/g, respectively whereas for MoS₂ the best fitting of Langmuir model was observed which means that the process of Cr(VI) adsorption at MoS₂ was homogenous adsorption and the highest adsorption capacities achieved at 298 K, 308 K and 318 K were 113.7 mg/g, 129.6 mg/g, and 144.9 mg/g respectively. The increase in K_f values with increasing temperature signifies that the adsorption capabilities improve with the rise in temperature [49]. Also, the values of other coefficients in the table such as $b > 0$ and $1/n$ ($0 < 1/n < 1$) depict the rapid capture of chromium ions on MXene and MoS₂. R_L values were also calculated to check the influence of temperature on Cr(VI) adsorption. All the R_L values are falling between 0 and 1 for both adsorbents which shows that the adsorption was favorable at all the three temperatures. The data in Table S5 summarizes the overall performance of MXene and MoS₂ adsorbents for Cr(VI) removal. The comparison in both materials highlights that MoS₂ shows good removal efficiencies for chromium removal as compared to MXene.

3.6. Thermodynamic investigation

To study the thermodynamic properties of the Cr(VI) adsorption on MXene and MoS₂, comparative analysis was performed at different temperatures of 298 K, 308 K and 318 K, at initial concentration of 30 mg/L and pH 2 (Table 1). It is worth mentioning that increase in temperature (298 K, 308 K, 318 K) increases the adsorption capacities of Cr(VI) for both MXene (26.8 mg/g, 27.6 mg/g, 29.7 mg/g) and MoS₂ (54.3 mg/g, 56.6 mg/g, 59.2 mg/g) shown in Fig. S5. Similar adsorption patterns for Cr(VI) adsorption were shown by [49,59]. Thermodynamic parameters, including entropy (ΔS°), enthalpy (ΔH°) changes, and Gibbs free energy (ΔG°), were calculated using the following equations:

$$K_c = Q_e/C_e \quad (21)$$

$$\Delta G^\circ = -RT \ln K_c \quad (22)$$

$$\ln K_c = (\Delta S^\circ/R) - (\Delta H^\circ/RT) \quad (23)$$

where K_c stands for equilibrium gas constant, R represents the ideal gas constant equal to 8.314 J/mol/K, T stands for temperature in Kelvin, and Q_e and C_e are the adsorption capacity of adsorbent and chromium concentration in the effluent, respectively.

ΔS° and ΔH° are determined from intercept and slope of the graph plotted $\ln K_c$ vs $1/T$ (Figs. 6C and 6D). The Cr(VI) adsorption increases with an increase in temperature. Greater positive values of ΔH° (23.469 kJ/mol for MXene and 48.322 kJ/mol for MoS₂) indicate that the process of adsorption on nanomaterials is endothermic and is promoted at increasing temperature. Additionally, the high degree of dislocations and disorder at Cr(VI) / MXene and Cr(VI) / MoS₂ interfaces are indicated by the positive values of ΔS° for MXene (0.0691 kJ/mol/K) and MoS₂ (0.171 kJ/mol/K), respectively [52].

3.7. Effect of coexisting ions on adsorption

Most of the inorganic ions are found in the industrial wastewater (Ca^{2+} , Mg^{2+} , Na^+ , PO_4^{3-} , HCO_3^{2-} , Cl^-) and the natural water sources are contaminated due to rapid industrialization [64]. Coexisting anions compete with Cr(VI) ions for occupying the active sites and decrease the removal percentage of Cr(VI). Therefore, to assess the efficiency of an adsorbent for selective adsorption performance, the effect of coexisting ions with concentration of ions 30 mg/L on Cr(VI) removal at MXene and MoS₂ were calculated, and the results are shown in Fig. 7.

Influence of three cations (Ca^{2+} , Mg^{2+} , Na^+) and three anions (PO_4^{3-} , HCO_3^{2-} , Cl^-) was studied on Cr(VI) removal using MXene Fig. 7A and MoS₂ Fig. 7B, respectively. From the above results it can be concluded that the positive ions had little competition with Cr(VI) ions as the adsorbents were positively charged in the acidic media which

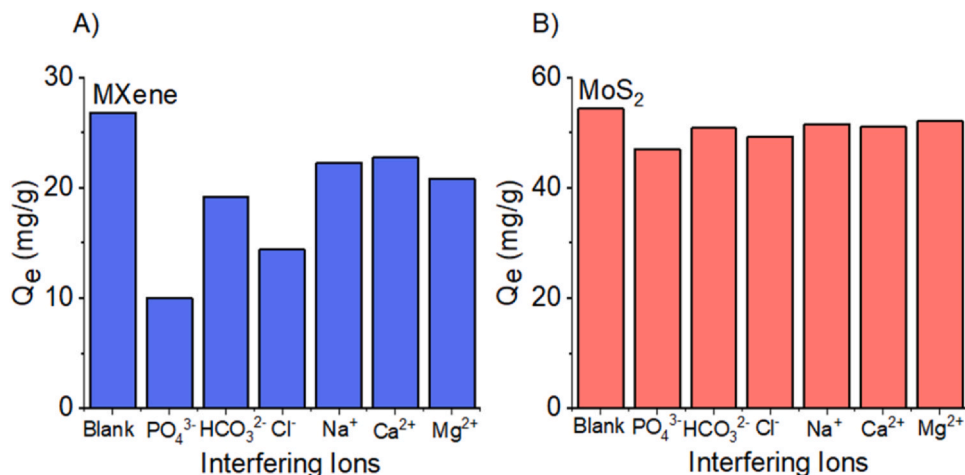


Fig. 7. Effect of coexisting ions on Cr(VI) adsorption by (A) MXene (Dosage = 1 g/L, T = 298 K, Time = 9 h, pH = 2, C_o = 30 mg/L) and (B) MoS₂ (Dosage = 0.5 g/L, T = 298 K, Time = 1.5 h, pH = 2, C_o = 30 mg/L).

avored electrostatic repulsion as compared to anions which showed more competitiveness due to the negative charge which was attracted by both adsorbents. In the case of MXenes, the competitiveness in the ability of anions for adsorption is shown maximum for PO₄³⁻ then comes the Cl⁻ and the least effect of HCO₃²⁻ is seen with Cr(VI) adsorption. The greater effect by PO₄³⁻ may be attributed to varying charge distribution and hydrated radii [49]. On the other hand, MoS₂ exhibits varying adsorption capacities with multiple ions coexisting with Cr(VI) ions in water. The effect of coexisting ions on Cr(VI) adsorption is not incredibly significant in the presence of MoS₂. The above results ensure the better selectivity of MoS₂ over MXene.

3.8. Reusability of MXene and MoS₂

To assess the practical application of adsorbents, it is significant to evaluate the reusability and recyclability of the materials. Therefore, regeneration experiments were conducted to check if the adsorbents can be reused for the Cr(VI) removal. For experimentation, 1 g/L of MXene and 0.5 g/L of MoS₂ were taken in 100 mL Cr(VI) solution at room temperature with chromium concentration 30 mg/L at pH 2.

Further, the materials were separated after adsorption and moved to 1 M NaOH solution. The MXene-Cr and MoS₂-Cr complex was agitated in 1 M NaOH solution for 8 h to desorb the adsorbed Cr species from the surface of adsorbents. MXene and MoS₂ were further washed with deionized water several times to attain neutral pH for conducting the next cycle. The regenerated adsorbents were dried overnight and used again for chromium adsorption. Fig. 8A and Fig. 8B show the

adsorption performance of MXene and MoS₂ respectively, after each cycle. MXene showed a decrease in removal percentage up to 70 % after fifth cycle whereas the decrease in percentage removal reached 79 % in case of MoS₂ after fifth cycle. The reduction in the removal efficiencies is attributed to the loss of adsorbent's mass and the number of active sites.

4. Conclusion

In this study, comparison of two emerging two-dimensional nano-materials was made and MoS₂ showed efficient adsorption capacities for Cr(VI) removal as compared to MXenes. MXenes and MoS₂ were utilized in unmodified form to better compare both the materials in water treatment applications. MoS₂ nanosheets performed well due to the addition of PVP in synthesis process. Different characterization techniques such as SEM, XRD, FTIR and BET confirmed the successful synthesis of MXene and MoS₂. The effect of adsorption parameters was also applied on both adsorbents to better understand the operating conditions and performance operators. Both the adsorbents showed better performance as compared to the conventional adsorbents, but this needs further modification to make the process efficient and faster. The analysis of adsorption data reveals the best fit of Langmuir model for MoS₂ and Freundlich model for MXene and the maximum adsorption capacities achieved for MXene and MoS₂ were 59.8 mg/g and 113.7 mg/g at 298 K, respectively. Furthermore, the process of adsorption was signified by the change in Gibbs free energy and enthalpy. The negative values of change in Gibbs free energy and positive values

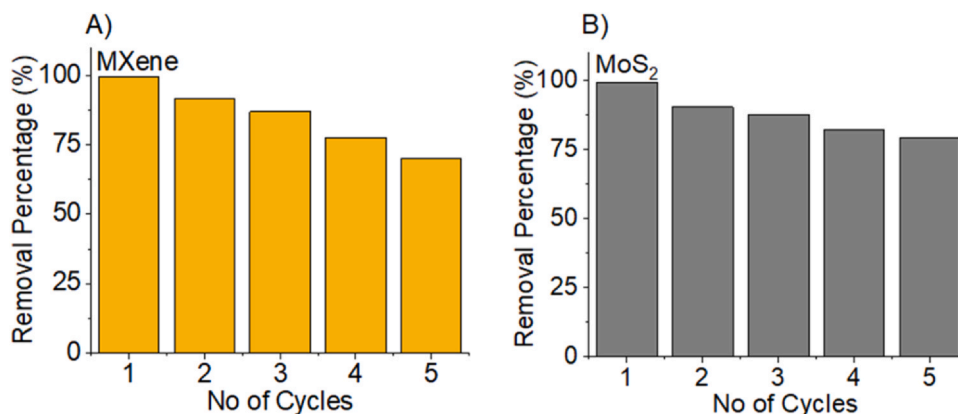


Fig. 8. Regeneration studies of MXenes (Dosage = 1 g/L, T = 298 K, Time = 9 h, pH = 2, C_o = 30 mg/L) and (B) MoS₂ (Dosage = 0.5 g/L, T = 298 K, Time = 1.5 h, pH = 2, C_o = 30 mg/L) for Cr(VI) adsorption.

of change in enthalpy confirm that the ongoing adsorption of both composites was spontaneous and endothermic in nature. The comparison study is a key index to highlight the properties of two-dimensional materials in water treatment applications. MXenes are arduous to handle for adsorption as they have less stability which retards its performance for heavy metal adsorption. Moreover, the research can also be extended for comparison of other two-dimensional adsorbents and the composites of two-dimensional nanomaterials. The study will pave a way for the treatment of multiple cations and anions present in industrial wastewater. The synergetic effect of both adsorbents will be a good approach to trap the negative ions of chromium. It can be convinced that both MXene and MoS_2 are potential adsorbents for heavy metal adsorption even in unmodified form and this potential can further be enhanced through multiple approaches of modification. To the best of our knowledge, this is the first comparative study conducted for Cr(VI) removal using MXene and MoS_2 without any surface modification. The higher removal efficiencies over conventional adsorbents at different time intervals suggests that MXene and MoS_2 can further be functionalized and manipulated with desired materials to improve their performances in water and wastewater treatment applications.

CRedit authorship contribution statement

Musharib Khan: Writing – review & editing, Resources, Formal analysis, Conceptualization. **Waheed Miran:** Writing – review & editing, Supervision, Conceptualization. **Waqas Qamar Zaman:** Writing – review & editing, Writing – original draft. **Asma Maqsood Abbasi:** Writing – original draft, Formal analysis, Data curation, Conceptualization. **Fahad Azad:** Writing – original draft, Methodology, Formal analysis. **Hassan Anwer:** Writing – original draft, Conceptualization. **Xizi Long:** Writing – review & editing, Validation.

Data availability

Data will be made available on request.

Declaration of Competing Interest

The authors declare that they have no known competing financial interests or personal relationships that could have appeared to influence the work reported in this paper.

Declaration of Generative AI and AI-assisted technologies in the writing process

During the preparation of this work the author(s) used chatgpt in order to improve the quality of English. After using this tool/service, the author(s) reviewed and edited the content as needed and take(s) full responsibility for the content of the publication.

Acknowledgments

The authors would like to acknowledge the financial support from National University of Sciences & Technology (NUST).

Appendix A. Supporting information

Supplementary data associated with this article can be found in the online version at [doi:10.1016/j.dwt.2024.100693](https://doi.org/10.1016/j.dwt.2024.100693).

References

- Xiang L, Niu C-G, Tang N, Lv X-X, Guo H, Li Z-W, et al. Polypyrrole coated molybdenum disulfide composites as adsorbent for enhanced removal of Cr(VI) in aqueous solutions by adsorption combined with reduction. *Chem Eng J* 2021;408:127281.
- Foroutan R, Peighambarioust SJ, Mohammadi R, Omidvar M, Sorial GA, Ramavandi B. Influence of chitosan and magnetic iron nanoparticles on chromium adsorption behavior of natural clay: adaptive neuro-fuzzy inference modeling. *Int J Biol Macromol* 2020;151:355–65.
- Peng H, Guo J. Removal of chromium from wastewater by membrane filtration, chemical precipitation, ion exchange, adsorption electrocoagulation, electrochemical reduction, electrodialysis, electrodeionization, photocatalysis and nanotechnology: a review. *Environ Chem Lett* 2020;18(6):2055–68.
- Georgaki M-N, Charalambous M, Kazakis N, Talias MA, Georgakis C, Papamitsou T, et al. Chromium in water and carcinogenic human health risk. *Environments* 2023;10(2):33.
- Boussouga Y-A, Okkali T, Luxbacher T, Schäfer AI. Chromium (III) and chromium (VI) removal and organic matter interaction with nanofiltration. *Sci Total Environ* 2023;885:163695.
- Konradt N, Dillmann S, Becker J, Schroden D, Rohns H-P, Wagner C, et al. Removal of chromium species from low-contaminated raw water by different drinking water treatment processes. *Water* 2023;15(3):516.
- de Borja Ojembarrena F, Sammarie H, Campano C, Blanco A, Merayo N, Negro C. Hexavalent chromium removal from industrial wastewater by adsorption and reduction onto cationic cellulose nanocrystals. *Nanomaterials* 2022;12(23):4172.
- Liu S, Gao J, Zhang L, Yang Y, Liu X. Diethylenetriaminepentaacetic acid-thiourearemodified magnetic chitosan for adsorption of hexavalent chromium from aqueous solutions. *Carbohydr Polym* 2021;274:118555.
- Prasad S, Yadav KK, Kumar S, Gupta N, Cabral-Pinto MM, Rezanian S, et al. Chromium contamination and effect on environmental health and its remediation: A sustainable approaches. *J Environ Manag* 2021;285:112174.
- Aslani H, Ebrahimi Kosari T, Naseri S, Nabizadeh R, Khazaei M. Hexavalent chromium removal from aqueous solution using functionalized chitosan as a novel nano-adsorbent: modeling and optimization, kinetic, isotherm, and thermodynamic studies, and toxicity testing. *Environ Sci Pollut Res* 2018;25:20154–68.
- Heidari A, Sayadi M, Biglari Quchan Atigh Z. A comparative study of different materials (drinking water treatment sludge, nanoclay, and modified nanoclay) for simultaneous removal of hexavalent chromium and lead. *Int J Environ Sci Technol* 2021:1–18.
- Georgaki M-N, Charalambous M. Toxic chromium in water and the effects on the human body: a systematic review. *J Water Health* 2023;21(2):205–23.
- Ukhurebor KE, Aigbe UO, Onyancha RB, Nwankwo W, Osibote OA, Paumo HK, et al. Effect of hexavalent chromium on the environment and removal techniques: a review. *J Environ Manag* 2021;280:111809.
- Yang W, Song W, Li J, Zhang X. Bioleaching of heavy metals from wastewater sludge with the aim of land application. *Chemosphere* 2020;249:126134.
- He PY, Zhang YJ, Chen H, Han ZC, Liu LC. Low-cost and facile synthesis of geopolymer-zeolite composite membrane for chromium (VI) separation from aqueous solution. *J Hazard Mater* 2020;392:122359.
- Shoneye A, Sen Chang J, Chong MN, Tang J. Recent progress in photocatalytic degradation of chlorinated phenols and reduction of heavy metal ions in water by TiO₂-based catalysts. *Int Mater Rev* 2022;67(1):47–64.
- Du J, Shang X, Shi J, Guan Y. Removal of chromium from industrial wastewater by magnetic flocculation treatment: experimental studies and PSO-BP modelling. *J Water Process Eng* 2022;47:102822.
- Zhao Y, Li L, Zuo Y, He G, Chen Q, Meng Q, et al. Reduced graphene oxide supported ZnO/CdS heterojunction enhances photocatalytic removal efficiency of hexavalent chromium from aqueous solution. *Chemosphere* 2022;286:131738.
- Shukrullah S, Azam M, Naz MY, Toqeer I, Gungor A. Effective removal of chromium from wastewater with Zn doped Ni ferrite nanoparticles produced using co-precipitation method. *Mater Today: Proc* 2021;47:S9–12.
- Wei S, Jia L, Tan J, Zhang J, Guo Z, Hu Z, et al. Iron-carbon micro-electrolysis simultaneously enhanced nutrient and heavy metal removal in constructed wetlands for purifying polluted groundwater with variable hydraulic loadings. *Chem Eng J* 2023;470:144367.
- Lei C, Wang C, Chen W, He M, Huang B. Polyaniline@ magnetic chitosan nanomaterials for highly efficient simultaneous adsorption and in-situ chemical reduction of hexavalent chromium: Removal efficacy and mechanisms. *Sci Total Environ* 2020;733:139316.
- Ren Y, Han Y, Lei X, Lu C, Liu J, Zhang G, et al. A magnetic ion exchange resin with high efficiency of removing Cr (VI). *Colloids Surf A: Physicochem Eng Asp* 2020;604:125279.
- Shigidi I, Anqi AE, Elkhaleefa A, Mohamed A, Ali IH, Brima EI. Temperature impact on reverse osmosis permeate flux in the remediation of hexavalent chromium. *Water* 2021;14(1):44.
- Singh A, Pal DB, Mohammad A, Alhazmi A, Haque S, Yoon T, et al. Biological remediation technologies for dyes and heavy metals in wastewater treatment: New insight. *Bioresour Technol* 2022;343:126154.
- Mahesh N, Balakumar S, Shyamalagowri S, Manjunathan J, Pavithra M, Babu PS, et al. Carbon-based adsorbents as proficient tools for the removal of heavy metals from aqueous solution: a state of art-review emphasizing recent progress and prospects. *Environ Res* 2022;213:113723.
- Santhosh C, Velmurugan V, Jacob G, Jeong SK, Grace AN, Bhatnagar A. Role of nanomaterials in water treatment applications: a review. *Chem Eng J* 2016;306:1116–37.
- Liu X, Ma R, Wang X, Ma Y, Yang Y, Zhuang L, et al. Graphene oxide-based materials for efficient removal of heavy metal ions from aqueous solution: A review. *Environ Pollut* 2019;252:62–73.
- Zuo X, Balasubramanian R. Evaluation of a novel chitosan polymer-based adsorbent for the removal of chromium (III) in aqueous solutions. *Carbohydr Polym* 2013;92(2):2181–6.
- Yu G, Lu Y, Guo J, Patel M, Bafana A, Wang X, et al. Carbon nanotubes, graphene, and their derivatives for heavy metal removal. *Adv Compos Hybrid Mater* 2018;1:56–78.

- [30] El-Mehalmey WA, Ibrahim AH, Abugable AA, Hassan MH, Haikal RR, Karakalos SG, et al. Metal-organic framework@ silica as a stationary phase sorbent for rapid and cost-effective removal of hexavalent chromium. *J Mater Chem A* 2018;6(6):2742–51.
- [31] Zhou L, Li R, Zhang G, Wang D, Cai D, Wu Z. Zero-valent iron nanoparticles supported by functionalized waste rock wool for efficient removal of hexavalent chromium. *Chem Eng J* 2018;339:85–96.
- [32] Guo T, Lei Y, Hu X, Yang G, Liang J, Huang Q, et al. Hydrothermal synthesis of MXene-MoS₂ composites for highly efficient removal of pesticides. *Appl Surf Sci* 2022;588:152597.
- [33] Anasori B, Gogotsi Y. The global expansion of MXenes. *Graph 2D Mater* 2023;8(3):39–41.
- [34] Karthikeyan P, Ramkumar K, Pandi K, Fayyaz A, Meenakshi S, Park CM. Effective removal of Cr (VI) and methyl orange from the aqueous environment using two-dimensional (2D) Ti₃C₂T_x MXene nanosheets. *Ceram Int* 2021;47(3):3692–8.
- [35] Shahzad A, Nawaz M, Mozahida M, Jang J, Tahir K, Kim J, et al. Ti₃C₂T_x MXene core-shell spheres for ultrahigh removal of mercuric ions. *Chem Eng J* 2019;368:400–8.
- [36] Ali MEM, Mohammed R, Abdel-Moniem SM, El-Liethy MA, Ibrahim HS. Green MoS₂ nanosheets as a promising material for decontamination of hexavalent chromium, pharmaceuticals, and microbial pathogen disinfection: spectroscopic study. *J Nanopart Res* 2022;24(10):191.
- [37] Guo Y, Li J. MoS₂ quantum dots: synthesis, properties and biological applications. *Mater Sci Eng: C* 2020;109:110511.
- [38] Abd-Elrahim A, Chun D-M. One-step mechanical exfoliation and deposition of layered materials (graphite, MoS₂, and BN) by vacuum-kinetic spray process. *Vacuum* 2022;196:110732.
- [39] Mei L, Cao Z, Ying T, Yang R, Peng H, Wang G, et al. Simultaneous electrochemical exfoliation and covalent functionalization of MoS₂ membrane for ion sieving. *Adv Mater* 2022;34(26):2201416.
- [40] Sahoo D, Kumar B, Sinha J, Ghosh S, Roy SS, Kaviraj B. Cost effective liquid phase exfoliation of MoS₂ nanosheets and photocatalytic activity for wastewater treatment enforced by visible light. *Sci Rep* 2020;10(1):10759.
- [41] Lu C, Luo M, Ge Y, Huang Y, Zhao Q, Zhou Y, et al. Layer-dependent nonlinear optical properties of WS₂, MoS₂, and Bi₂S₃ films synthesized by chemical vapor deposition. *ACS Appl Mater* 2021;14(1):2390–400.
- [42] Yuan W, Kuang J, Yu M, Huang Z, Zou Z, Zhu L. Facile preparation of MoS₂@ Kaolin composite by one-step hydrothermal method for efficient removal of Pb (II). *J Hazard Mater* 2021;405:124261.
- [43] Jin L, Chai L, Yang W, Wang H, Zhang L. Two-dimensional titanium carbides (Ti₃C₂T_x) functionalized by poly (m-phenylenediamine) for efficient adsorption and reduction of hexavalent chromium. *Int J Environ Res Public Health* 2020;17(1):167.
- [44] Kong A, Sun Y, Peng M, Gu H, Fu Y, Zhang J, et al. Amino-functionalized MXenes for efficient removal of Cr (VI). *Colloids Surf A: Physicochem Eng Asp* 2021;617:126388.
- [45] Sun H, Wu T, Zhang Y, Ng DH, Wang G. Structure-enhanced removal of Cr (vi) in aqueous solutions using MoS₂ ultrathin nanosheets. *N J Chem* 2018;42(11):9006–15.
- [46] Jamaluddin NS, Alias NH, Samitsu S, Othman NH, Jaafar J, Marpani F, et al. Efficient chromium (VI) removal from wastewater by adsorption-assisted photocatalysis using MXene. *J Environ Chem Eng* 2022;10(6):108665.
- [47] Liu H, Chen X, Deng L, Su X, Guo K, Zhu Z. Preparation of ultrathin 2D MoS₂/ graphene heterostructure assembled foam-like structure with enhanced electrochemical performance for lithium-ion batteries. *Electrochim Acta* 2016;206:184–91.
- [48] Wang J, Zhang R, Huo Y, Ai Y, Gu P, Wang X, et al. Efficient elimination of Cr (VI) from aqueous solutions using sodium dodecyl sulfate intercalated molybdenum disulfide. *Ecotoxicol Environ Saf* 2019;175:251–62.
- [49] Xiang L, Niu C-G, Tang N, Lv X-X, Guo H, Li Z-W, et al. Polypyrrole coated molybdenum disulfide composites as adsorbent for enhanced removal of Cr (VI) in aqueous solutions by adsorption combined with reduction. *Chem Eng J* 2021;408:127281.
- [50] He L, Huang D, He Z, Yang X, Yue G, Zhu J, et al. Nanoscale zero-valent iron intercalated 2D titanium carbides for removal of Cr (VI) in aqueous solution and the mechanistic aspect. *J Hazard Mater* 2020;388:121761.
- [51] Chen M, Guo Q, Cui J, Lv W, Yao Y. Enhanced sorption and reduction of Cr (VI) by the flowerlike nanocomposites combined with molybdenum disulfide and polypyrrole. *Environ Technol* 2022;43(18):2796–808.
- [52] Wang J, Wang X, Zhao G, Song G, Chen D, Chen H, et al. Polyvinylpyrrolidone and polyacrylamide intercalated molybdenum disulfide as adsorbents for enhanced removal of chromium (VI) from aqueous solutions. *Chem Eng J* 2018;334:569–78.
- [53] Cai W, Dionysiou DD, Fu F, Tang B. CTAB-intercalated molybdenum disulfide nanosheets for enhanced simultaneous removal of Cr (VI) and Ni (II) from aqueous solutions. *J Hazard Mater* 2020;396:122728.
- [54] Feng Y, Wang H, Xu J, Du X, Cheng X, Du Z, et al. Fabrication of MXene/PEI functionalized sodium alginate aerogel and its excellent adsorption behavior for Cr (VI) and Congo Red from aqueous solution. *J Hazard Mater* 2021;416:125777.
- [55] Zeng X, Wang Y, He X, Liu C, Wang X, Wang X. Enhanced removal of Cr (VI) by reductive sorption with surface-modified Ti₃C₂T_x MXene nanocomposites. *J Environ Chem Eng* 2021;9(5):106203.
- [56] Baig MM, Pervaiz E, Yang M, Gul IH. High-performance supercapacitor electrode obtained by directly bonding 2D materials: hierarchal MoS₂ on reduced graphene oxide. *Front Mater* 2020;7:580424.
- [57] Wang H, Cui H, Song X, Xu R, Wei N, Tian J, et al. Facile synthesis of heterojunction of MXenes/TiO₂ nanoparticles towards enhanced hexavalent chromium removal. *J Colloid Interface Sci* 2020;561:46–57.
- [58] Yang G, Hu X, Liang J, Huang Q, Dou J, Tian J, et al. Surface functionalization of MXene with chitosan through in-situ formation of polyimidazoles and its adsorption properties. *J Hazard Mater* 2021;419:126220.
- [59] Shahzad A, Rasool K, Miran W, Nawaz M, Jang J, Mahmoud KA, et al. Two-dimensional Ti₃C₂T_x MXene nanosheets for efficient copper removal from water. *ACS Sustain Chem Eng* 2017;5(12):11481–8.
- [60] Harijan DK, Chandra V. Polyaniline functionalized graphene sheets for treatment of toxic hexavalent chromium. *J Environ Chem Eng* 2016;4(3):3006–12.
- [61] Jun B-M, Heo J, Taheri-Qazvini N, Park CM, Yoon Y. Adsorption of selected dyes on Ti₃C₂T_x MXene and Al-based metal-organic framework. *Ceram Int* 2020;46(3):2960–8.
- [62] Fard AK, Mckay G, Chamoun R, Rhadfi T, Preud'Homme H, Atieh MA. Barium removal from synthetic natural and produced water using MXene as two dimensional (2-D) nanosheet adsorbent. *Chem Eng J* 2017;317:331–42.
- [63] Abin-Bazaine A, Trujillo AC, Olmos-Marquez M. Adsorption Isotherms: Enlightenment of the Phenomenon of Adsorption. *Wastewater Treatment. IntechOpen*; 2022.
- [64] Shahzad A, Jang J, Lim S-R, Lee DS. Unique selectivity and rapid uptake of molybdenum-disulfide-functionalized MXene nanocomposite for mercury adsorption. *Environ Res* 2020;182:109005.